

AD-753 481

SEAWATER TEMPERATURE MEASUREMENT
FROM RAMAN SPECTRA

Chin H. Chang, et al

Avco Everett Research Laboratory, Incorporated

Prepared for:

Advanced Research Projects Agency
Naval Air Development Center

December 1972

DISTRIBUTED BY:

NTIS

National Technical Information Service
U. S. DEPARTMENT OF COMMERCE
5285 Port Royal Road, Springfield Va. 22151

AD753481

INTERIM TECHNICAL REPORT

SEAWATER TEMPERATURE MEASUREMENT
FROM RAMAN SPECTRA

Avco Everett Research Laboratory, Inc.
Everett, Massachusetts 02149
(617-389-3000)

Chin H. Chang and Lee A. Young, Principal Investigators

December 1972

Sponsored by

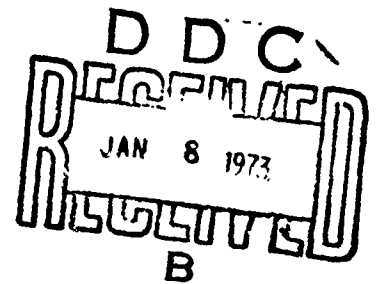
Advanced Research Projects Agency
ARPA Order No. 2194

Monitored by

Naval Air Development Center
Johnsville, Warminster, Pennsylvania 18974
Mr. Gerald Ferguson, AEYE/AETD, Project Engineer

Contract No: N62269-73-C-0073
Amount: \$98,500
Effect date: 31 August 1972
Expiration date: 31 March 1973

Reproduced by
NATIONAL TECHNICAL
INFORMATION SERVICE
U S Department of Commerce
Springfield VA 22151



DISTRIBUTION STATEMENT A
Approved for public release;
Distribution Unlimited

51

SUMMARY

Raman spectra of water have been measured in the laboratory using improved optical instrumentation. The linear depolarization ratio agrees well with results found in the literature. Various portions of the isotropic and anisotropic components of the Raman spectra can be identified with distinct structural species in liquid water. This model predicts that the depolarization will be most temperature dependent in the long-wavelength portion of the spectrum, as is demonstrated by our data. The measured linear depolarization ratio varies by 1.3% per degree centigrade; we predict that the temperature dependence of the circular depolarization ratio will be 1.7% / °C. The circular depolarization ratio is also a desirable indicator of temperature because of its value of ~ 0.67, leading to higher statistical accuracy in the cross-polarized channel, compared with ~ 0.25 for the linear depolarization ratio. Systematic measurements of the effect of temperature and salinity upon the circular depolarization will be undertaken shortly.

Variability of the spectral attenuation of light in seawater indicates that a two-color Raman technique is not feasible for use in the ocean. The circular depolarization ratio is to be preferred, provided that light is not appreciably depolarized further during transmission through seawater. To check this, the depolarization of light scattered through small angles has been measured in the laboratory, and found to be small but not negligible. Extrapolating the results to ocean conditions, we predict that

these effects can be corrected for to the required accuracy provided that seawater exhibits a fairly consistent relationship between depolarization and turbidity (which would be measured from the intensity of the Raman return). Preparations are now being made for field measurements of this relationship.

1. INTRODUCTION

The possibility of measuring subocean water temperature remotely by observing the Raman spectrum backscattered from a laser beam has been investigated in this laboratory. During the initial six months of this program under Contract N62269-72-C-0204, emphasis was on a two-color scheme in which the temperature sensitivity of the intensity ratio at two properly chosen Raman wavelengths was measured. Although it was concluded that a precision of about 0.2°C could be achieved by the two-color method down to a depth of 30 meters in clear ocean water¹ having constant optical characteristics, variations in the spectral attenuation coefficient of seawater would introduce serious errors in the temperature measurement. It is therefore desirable to investigate further the cross-polarization scheme which was found to be temperature sensitive in our previous measurements.

The construction of an improved back-scattering Raman spectrometer for this purpose, measurements of high resolution Raman spectra, isotropic and anisotropic components and depolarization ratios, and a new structural model of liquid water are discussed in this report.

The results show that the ratio of two polarization components of Raman radiation is an even more sensitive indicator of water temperature than the ratio of two-color intensities.

The results are preliminary. Systematic measurement of polarization ratios as functions of Raman wavelength, temperature and salinity will be undertaken shortly and presented in the final technical report.

2. LABORATORY MEASUREMENTS OF RAMAN SPECTRA

2.1 Improved Back-Scattering Raman Spectrometer

The improved version of our back-scattering Raman spectrometer is shown in Fig. 1. The laser radiation from the dye module is polarized perpendicularly to the scattering plane by a polarizing cube. After passing through a 100 \AA filter, which is centered about the laser wavelength, and a beam splitter, it is reflected by a small mirror, focused into the constant temperature ($\pm 0.1^\circ\text{C}$) Raman cell and eventually absorbed in the light trap.

Raman light is collected by the same focusing lens and its parallel and perpendicular polarization components are selected by properly rotating a second polarization cube. Since the $3/4$ - meter Spex monochromator grating has different efficiencies in the two planes of polarization, a Hanle quartz depolarizer (supplied by Karl Feuer Optical Associates, Inc. of Upper Montclair, N. J.) was placed in front of the Raman focusing lens thus avoiding the necessity of calibrating the grating separately for each mode of polarization. Signals from the diode, which monitors the laser intensity, and the PM tube on the monochromator are integrated and amplified by charge-sensitive preamplifiers and amplifiers. The total integrated charges are measured by the combination of amplitude encoders and pulse counters. To minimize the effect of dark current from the PM tube a coincidence pulse from a delay pulse generator synchroized by the N_2 laser is supplied to the encoders. A pulse

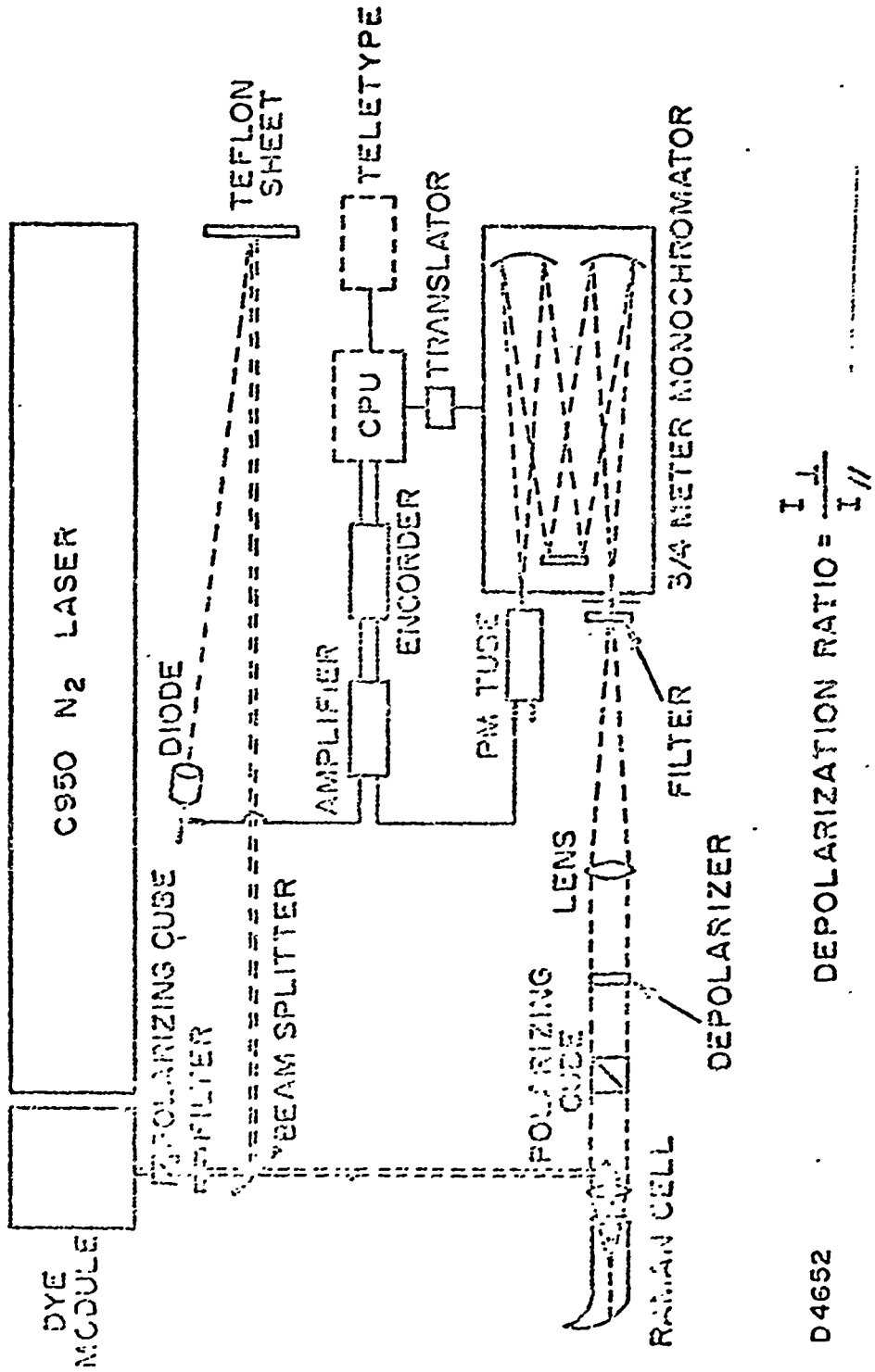


Fig. 1 Improved back-scattering Raman spectrometer.

generator is used to drive the stepping motor of the monochromator for a constant wavelength increment.

2.2 High Resolution Raman Spectrum of Water at 25°C

In order to investigate the polarization properties of the Raman spectrum of liquid water and hence their application to the remote measurement of water temperature, high resolution Raman spectra of water were measured with a well-tuned laser output of 3.0 Å⁰ spectral width and a monochromator band pass of 5.5 Å⁰ (15 cm⁻¹). Raman intensities were taken at 5 Å⁰ increments. An unpolarized total Raman spectrum of liquid H₂O in the OH stretching region is shown in Fig. 2. Fine features of the spectrum are in excellent agreement with the spectrum reported by Walrafen².

For the measurement of polarized components of the Raman spectrum of water, the scattering geometry is shown in Fig. 3. The exciting laser is polarized perpendicularly to the scattering plane containing both the laser and Raman axes. To simulate the field experiment, we are interested primarily in the back-scattering mode of the Raman process where the scattering angle $\theta = 0^\circ$. In this particular mode, the scattered Raman radiation can be polarized in the Z and X directions (Fig. 3), parallel and perpendicular respectively to the polarization of the laser. To correlate the laboratory measured intensity and the molecular polarizability tensor α which connects the applied field with the induced dipole by $|u| = \bar{\alpha} |e|$ in the liquid, one has to average over all possible molecular orientations with respect to the laboratory coordinate system.

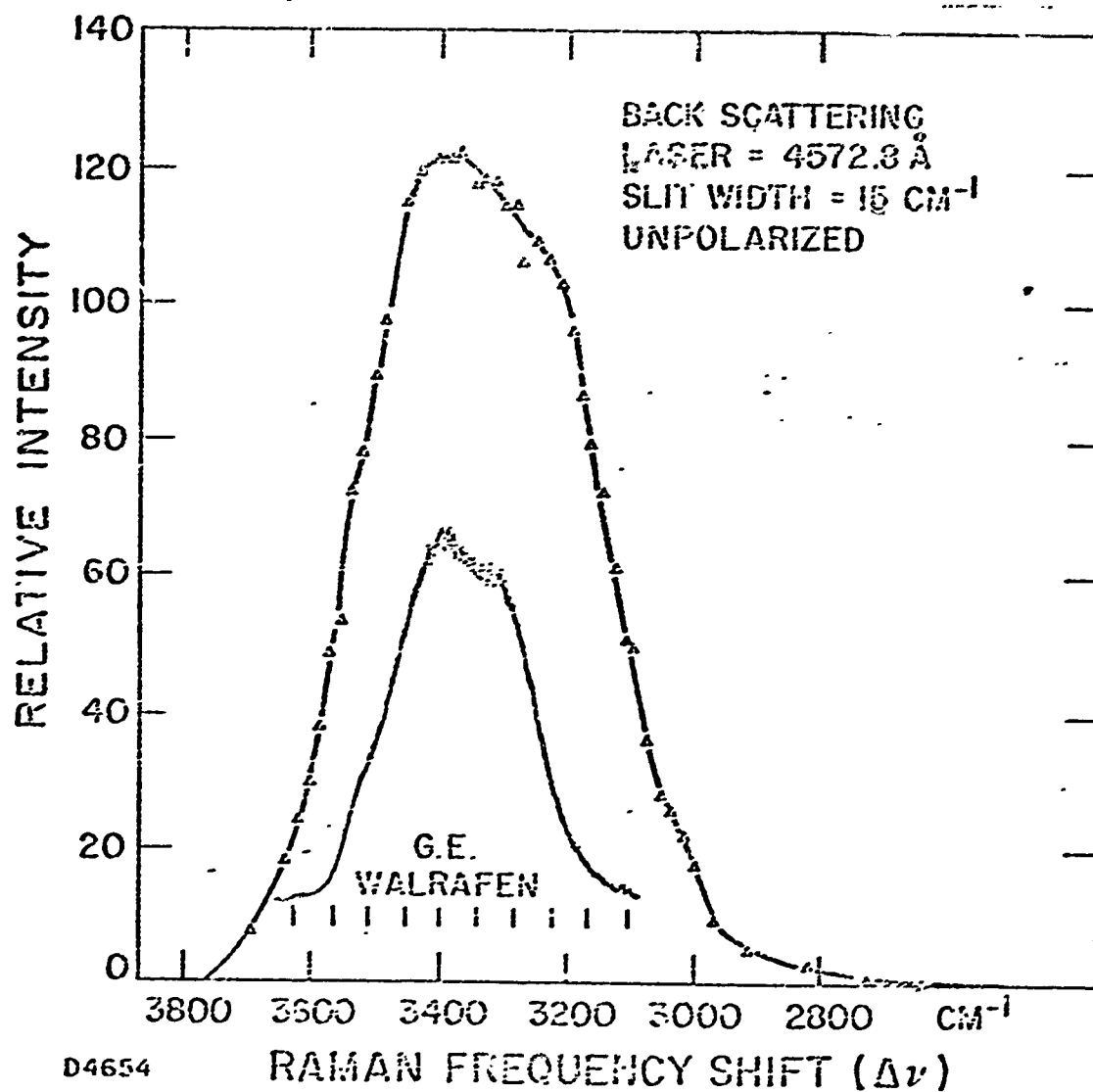
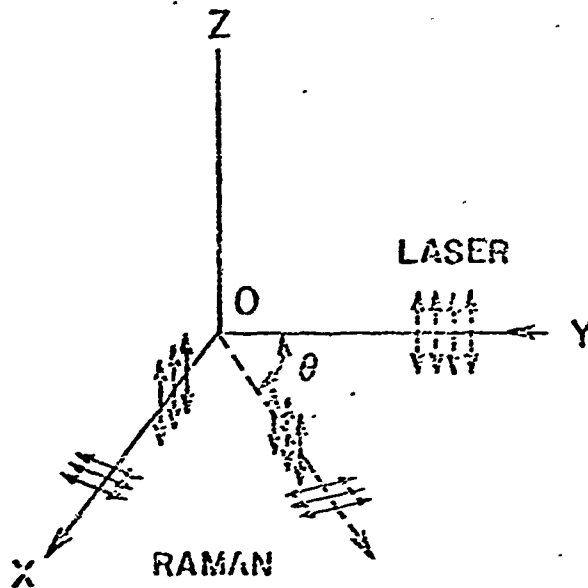


Fig. 2 Raman spectrum of liquid H₂O in the OH stretching region.



DEPOLARIZATION RATIO $\rho_i = \frac{I_{\perp}}{I_{\parallel}} = \frac{3\beta^2}{45\alpha^2 + 4\beta^2}$

ISOTROPIC COMPONENT $\propto 45\alpha^2$

ANISOTROPIC COMPONENT $\propto 3\beta^2$

D4651

Fig. 3 Scattering geometry used to specify the depolarization ratio and Raman components.

It is possible to show³ that the parallel (I_{\parallel}) and perpendicular (I_{\perp}) components of the measured intensity can be expressed as

$$I_{\parallel} = k(45a^2 + 4\beta^2) \quad (1)$$

and

$$I_{\perp} = k(3\beta^2), \quad (2)$$

where

$$a = \frac{1}{3} (a'_1 + a'_2 + a'_3) \quad (3)$$

$$\beta^2 = \frac{1}{2} [(a'_1 - a'_2)^2 + (a'_2 - a'_3)^2 + (a'_3 - a'_1)^2] \quad (4)$$

and k is the proportionality constant, a^2 is the so-called isotropic part of the differential polarizability tensor, β^2 is the anisotropy of the tensor and a'_1, a'_2, a'_3 are the principal values of the derivatives of the diagonalized molecular polarizability tensor which can be obtained by properly choosing the molecular axes.

Both parallel (\parallel) and perpendicular (\perp) components of the Raman spectrum of water at 25°C are shown in Fig. 4. As in the case of the unpolarized spectrum, measured intensities were corrected for the spectral sensitivity of the filters, grating and photomultiplier tube. Following a procedure similar to that of Scherer, Kint and Bailey⁴, a more meaningful display of Raman spectrum can be achieved by plotting the anisotropic and isotropic Raman spectra which are proportional to $3\beta^2$ and $45a^2$ respectively. This is done simply by means of equations (5) and (6):

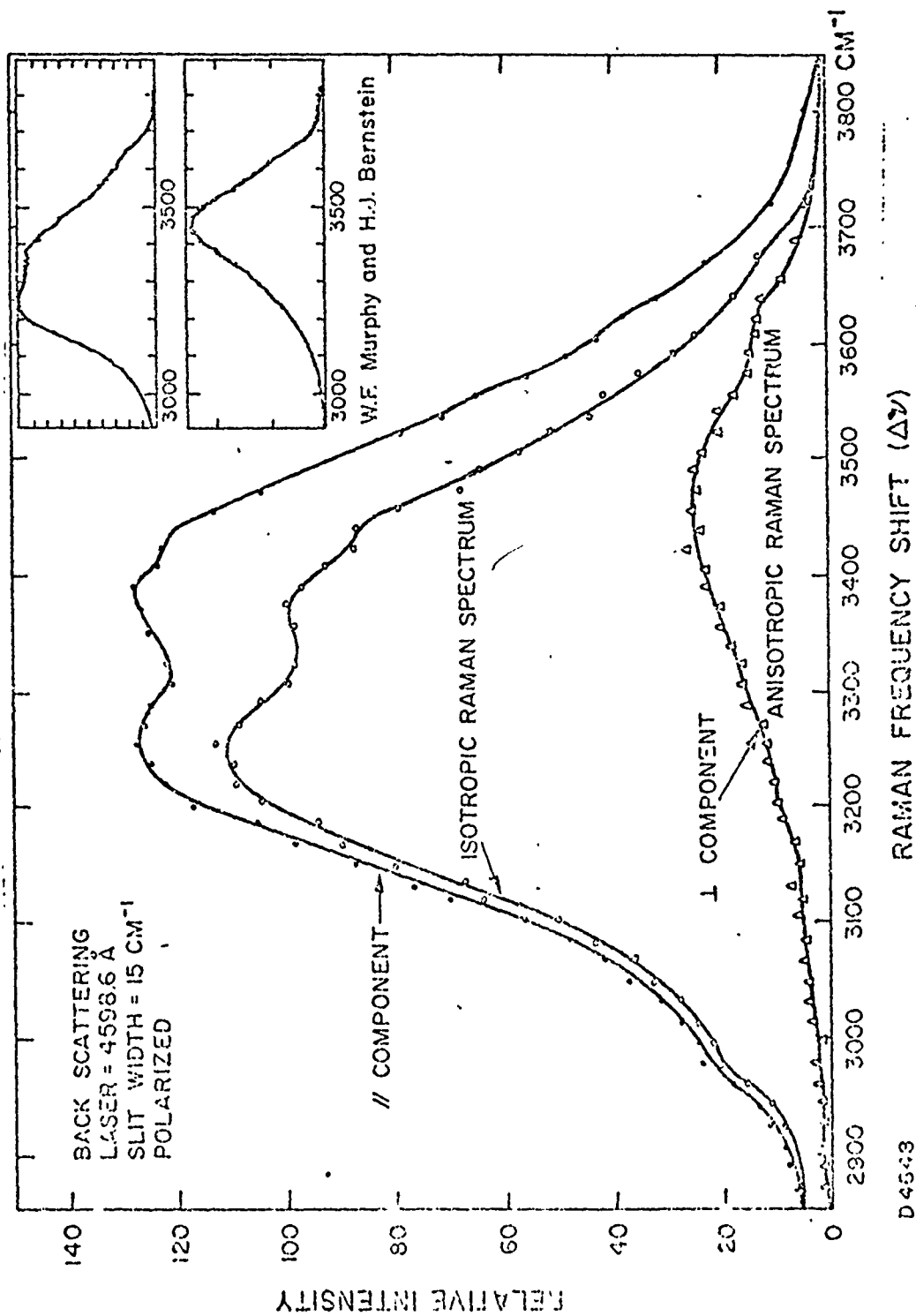


Fig. 4 Raman components of liquid H₂O in the OH stretching region.

$$I_{\text{aniso}} = I_{\perp} = k (3\beta^2) \quad (5)$$

$$I_{\text{iso}} = I_{\parallel} - \frac{4}{3} I_{\perp} = k(45\alpha^2) \quad (6)$$

Results of isotropic and anisotropic Raman spectra of water agree well with those reported most recently by Murphy and Bernstein⁵ as shown in Fig. 4.

The ratio of intensities of the perpendicular and parallel components is, by definition, the depolarization ratio, ρ_1 . From equations (1) and (2) this can be expressed as

$$\rho_1 = \frac{I_{\perp}}{I_{\parallel}} = \frac{3\beta^2}{45\alpha^2 + 4\beta^2} \quad (7)$$

Results of our depolarization ratio measurements for Raman back-scattering of water at room temperature shown in Fig. 5 compare well with those published^{5,6} for a 90° scattering angle. This result agrees with the theoretical prediction³ that the linear depolarization ratio is independent of scattering angle provided that the incident beam is polarized perpendicular to the scattering plane as it is in the cases reported here.

2.3 Molecular Model of Liquid Water and the Temperature Sensitivity of the Depolarization Ratio

Unlike water vapor, which is mostly monomeric with a simple structure, and the solid state (ice) which is highly ordered and whose

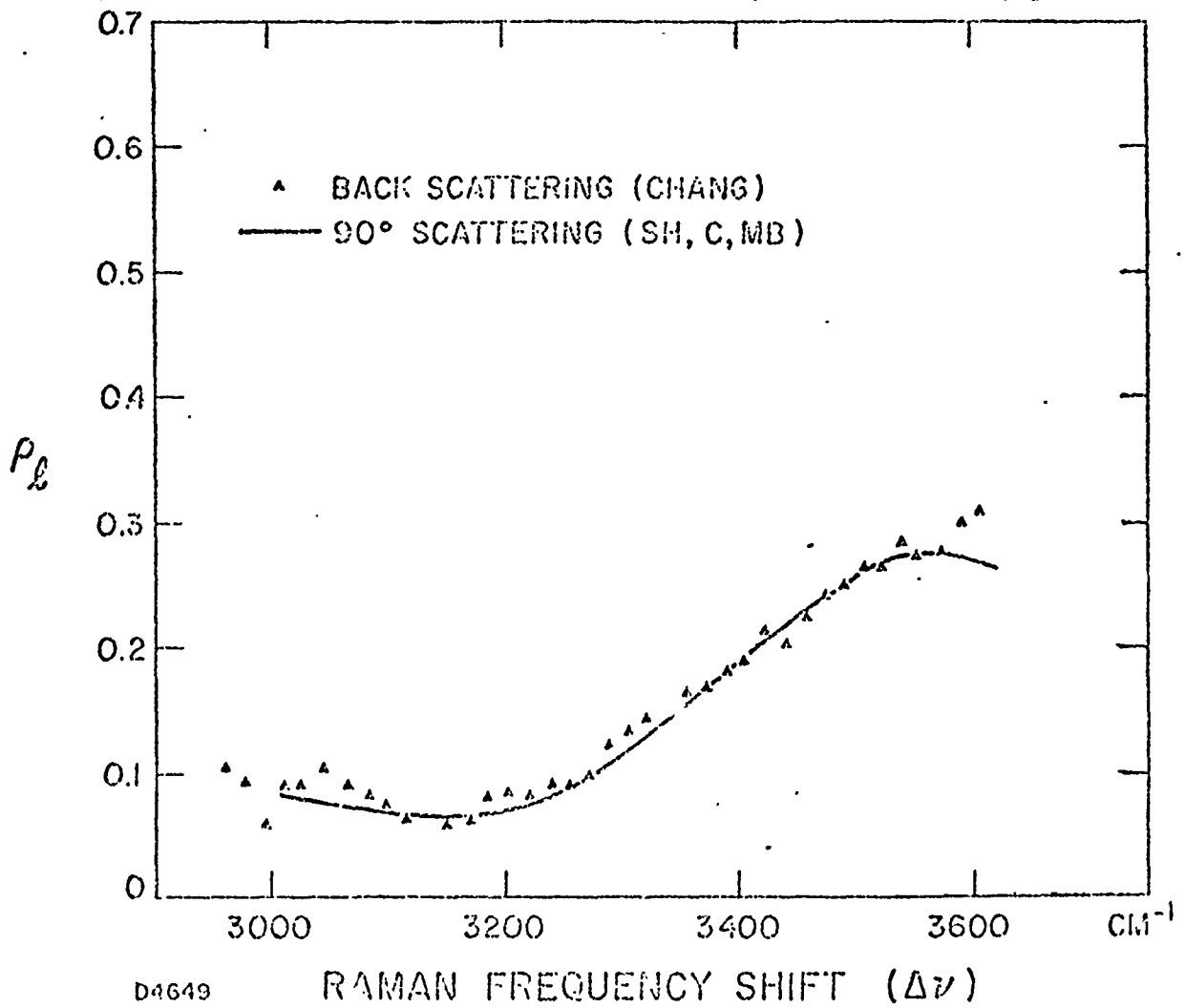


Fig. 5 Depolarization ratio in the OH stretching region of H₂O .
 SH, Reference 6a; C, Reference 6b; MB, Reference 5.

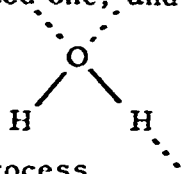
structure has been adequately characterized, the structure of liquid water remains a confused and controversial subject. The anomalous physical-chemical properties of liquid water have been interpreted as a result of hydrogen bonding which links water molecules together and is now fairly well understood. The geometrical configuration in which water molecules stick together by the hydrogen bond, however, is quite a different matter. The many models of the structure of liquid water which have been proposed from different point of view can be classified as (1) continuum or (2) mixture models. While the first kind of model postulates that the molecular structure of water changes continuously⁷ from ice-like at one extreme to gas-like at the other, the second category of model assumes the simultaneous existence of two or more distinguishable species of water⁸. Since our primary concern is the remote measurement of seawater temperature by means of Raman scattering, we restrict ourselves to the consideration of a two-species mixture model which has been successful in interpreting earlier sound absorption measurements⁹ and many recent infrared¹⁰, near-infrared¹¹ and Raman^{5, 12} spectroscopic studies. In this model, a kinetic equilibrium exist between two spectroscopically distinct structural species in liquid water.

A single water molecule in the liquid state, H_2O , is capable of forming a maximum of four hydrogen bonds through its hydrogen atoms and the two lone pairs of electrons on the oxygen atom. Since the average hydrogen bond energy has been estimated to be several kilocalories per mole^{11a, 13}, it is reasonable to speculate that no more than one hydrogen bond is broken at ordinary temperatures (0 - 40°C). Liquid water may

therefore be considered⁵ to be a mixture of two basic species:

H₂O molecules which are tetracoordinated through hydrogen bonds with four other H₂O units, and H₂O molecules which have only three hydrogen bonds (tricoordinated) as illustrated in Fig. 6. The dotted lines indicate hydrogen bonds in contrast to the ordinary OH chemical bonds which are shown by short solid lines. When a hydrogen bond linking two tetracoordinated H₂O units is broken by the thermal energy, two different

tricoordinated species are formed: (1) a species with both hydrogen atoms hydrogen bonded which is not spectroscopically distinguishable from the tetracoordinated one, and (2) a spectroscopically distinct species with one free O-H,



, whose formation is the net effect of the bond-breaking process.

Because of the internal motion, the tetracoordinated species can be assumed to have approximate C_{2v} symmetry^{5, 14}. The OH stretching vibrations may thus be classified as symmetric (ν_1) and asymmetric (ν_3) modes as in the free gaseous water molecule except both vibrational frequencies are expected to be lower in the tetracoordinated species since the OH bond is weakened by the hydrogen bond. Since only totally symmetric vibrations give polarized Raman lines ($\rho_1 < .25$) and others are depolarized ($\rho_1 = .75$)¹⁵, the symmetric mode is expected to be highly polarized ($\rho_1 < .25$) while the asymmetric mode should be completely depolarized ($\rho_1 = .75$) as predicted from group theoretical arguments. With the introduction of Fermi resonance between the overtone of the bending frequency at $1640 \pm 5 \text{ cm}^{-1}$ and the ν_1 mode, which splits the ν_1

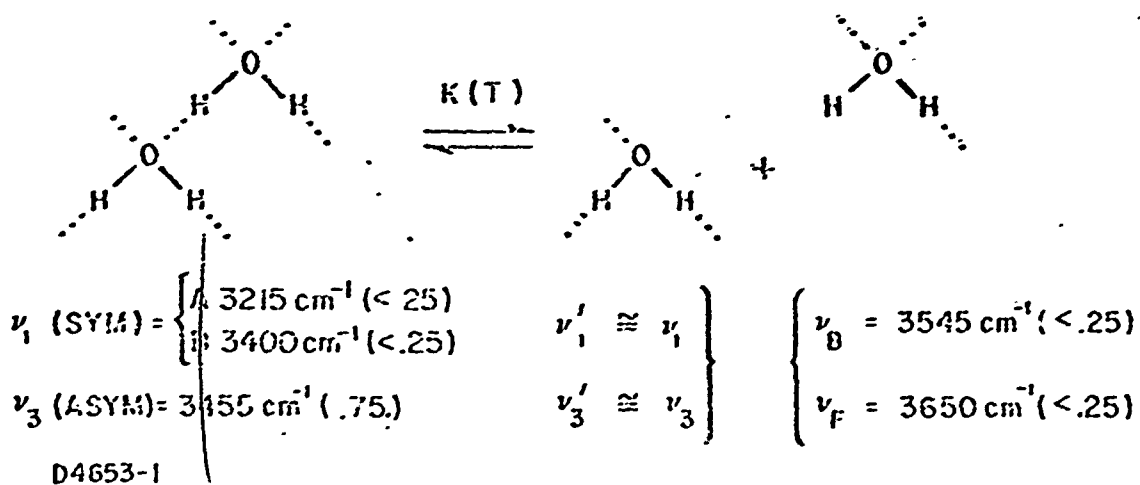
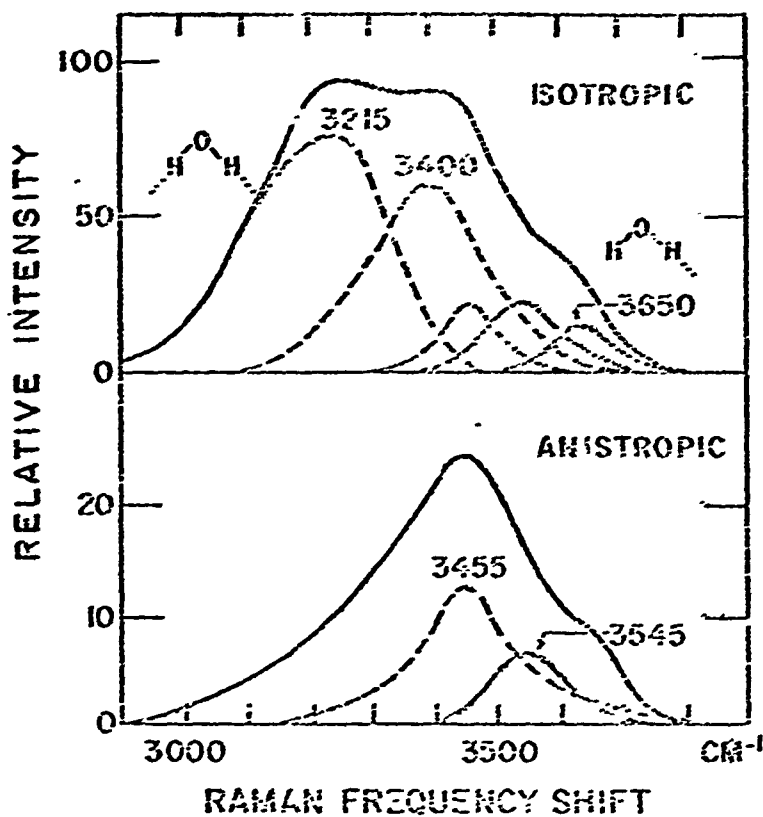
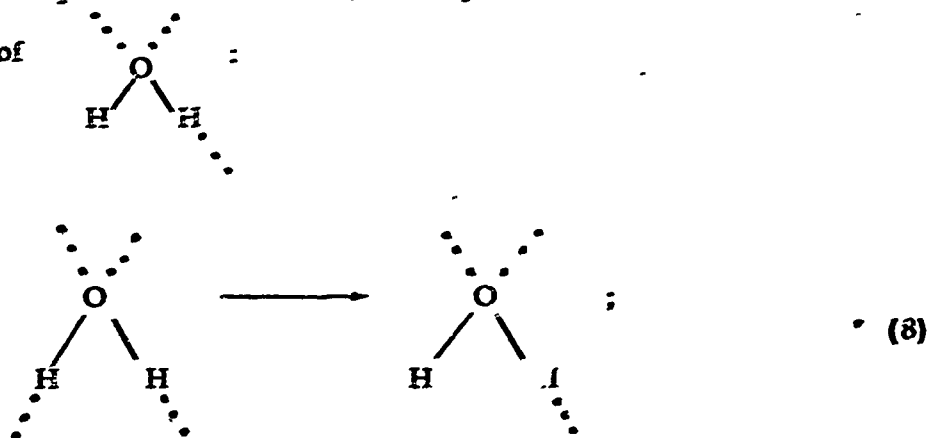


Fig. 6 Raman spectrum and the molecular structure of liquid water.

bond into ν_{1A} and ν_{1B} , reasonable assignments of OH stretching frequencies have been made by Murphy and Bernstein⁵ as shown in Fig. 6.

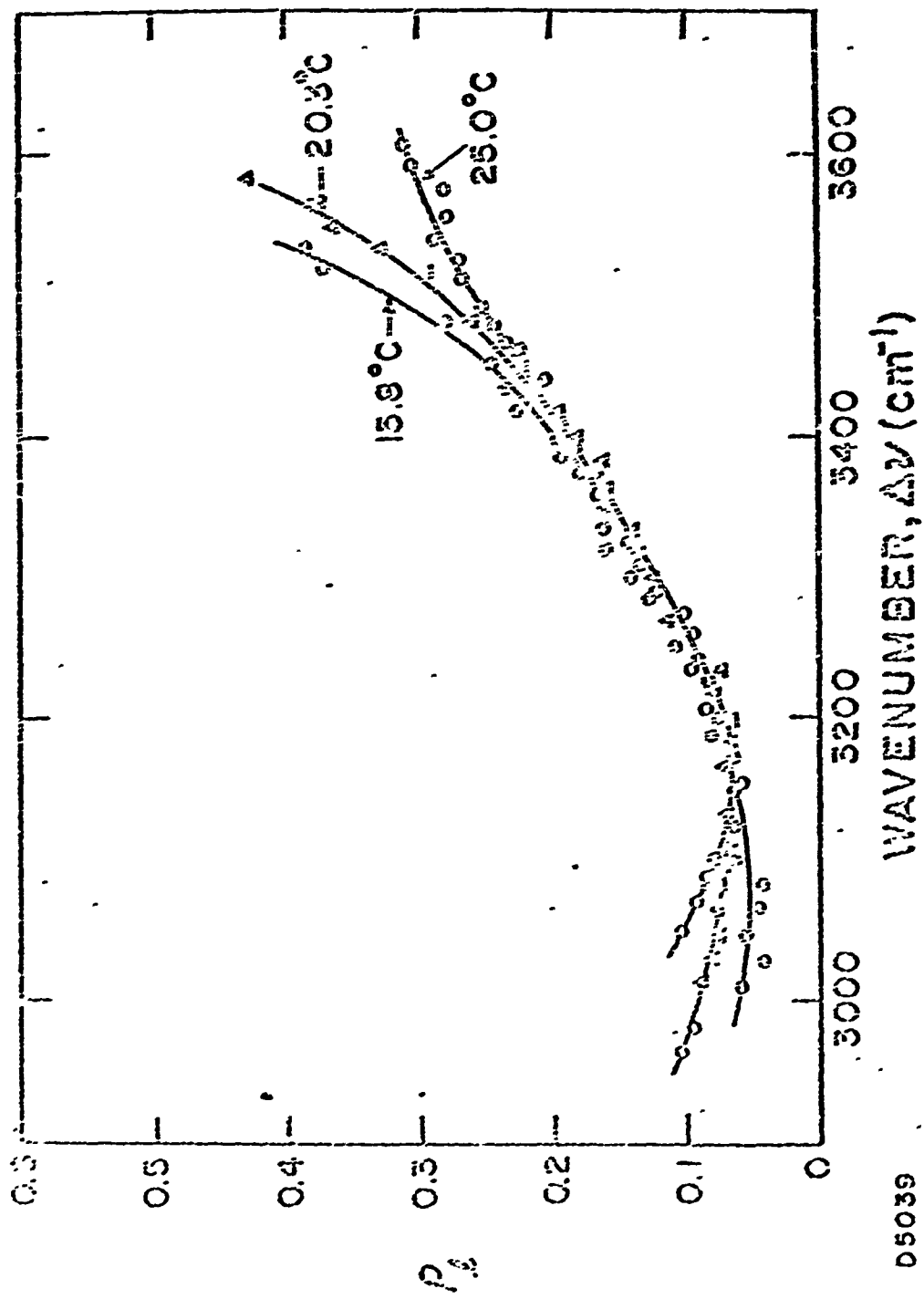
As the temperature increases, the equilibrium will be in favor of the formation of



therefore intensities at larger Raman frequency shifts in both isotropic and anisotropic components will be increased. Both the parallel and perpendicular components at high frequency will also increase with temperature.

On the other hand, since only the asymmetric ν_3 band is expected to be completely depolarized, at frequencies higher than 3450 cm^{-1} where the 3455 cm^{-1} and 3545 cm^{-1} bands mix the depolar-

ization ratio will be decreased as the temperature increases. Preliminary results from the temperature effect on the depolarization ratio of water at different temperatures are shown in Figs. 7 and 8. Besides data at frequencies lower than 3100 cm^{-1} where Raman intensities are low and thus uncertainties are high, the model presented here is successful in interpreting the temperature effect on the depolarization ratios. Although measurements are only preliminary, the temperature sensitivity of the linear depolarization ratio is most encouraging. On the basis of our data



05039

Fig. 7 Depolarization ratio for water.

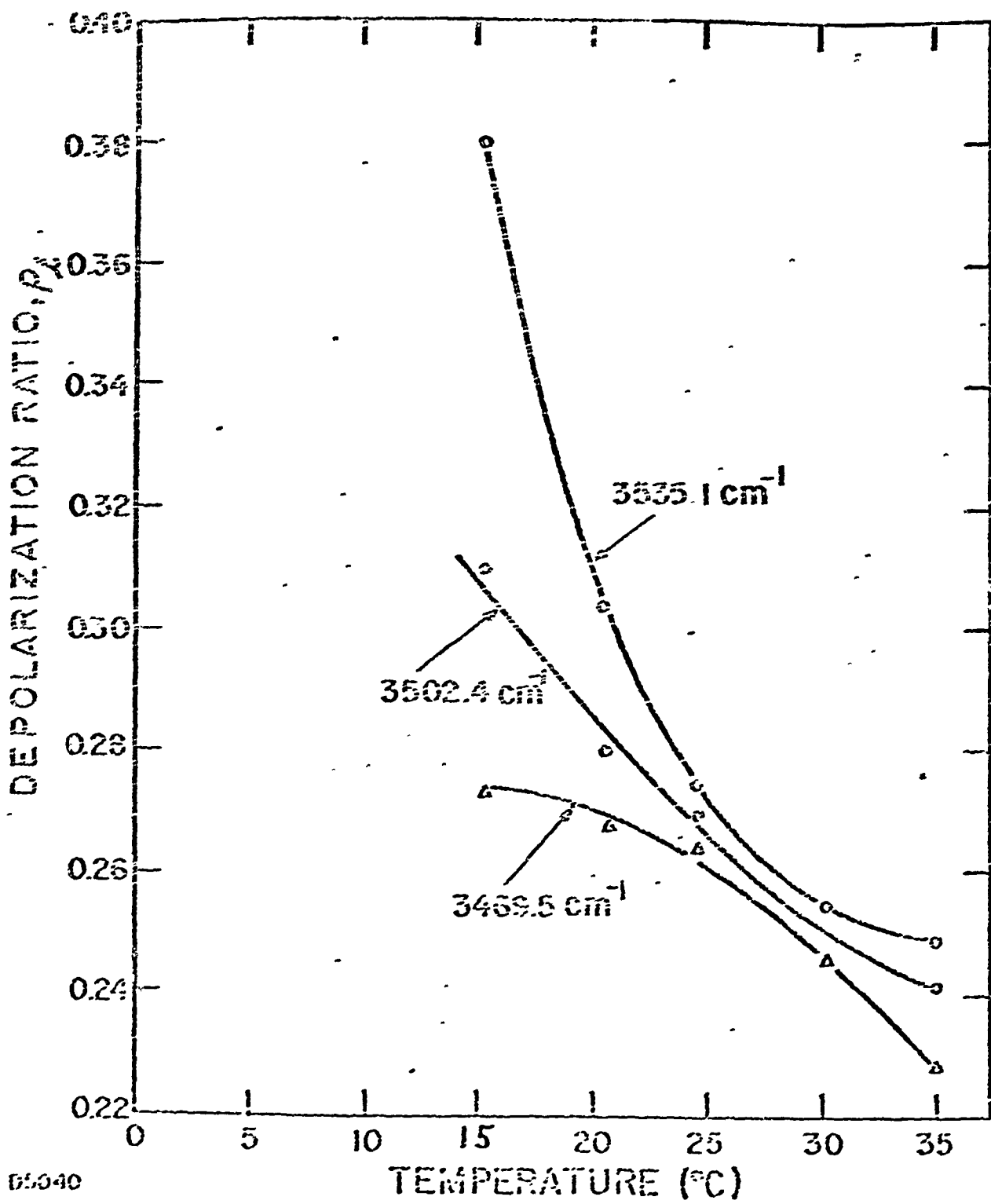


Fig. 8 Depolarization ratio for water at different temperatures.

(Fig. 8), the temperature sensitivity $\frac{d\rho_1/\rho_1}{dT}$ is found to be about $1.3\%/^{\circ}\text{C}$ at Raman shift of 3535 cm^{-1} . Since the circular depolarization ratio (ρ_c) can be related to linear ratio (ρ_1) by the following equation,¹⁶

$$\rho_c = \frac{2\rho_1}{1-\rho_1} \quad (9)$$

the temperature sensitivity can be estimated to be $1.7\%/^{\circ}\text{C}$ through equation (10),

$$\frac{d\rho_c/\rho_c}{dT} = \frac{1}{1-\rho_1} \cdot \frac{d\rho_1/\rho_1}{dT} \quad (10)$$

and values of $\frac{d\rho_1/\rho_1}{dT}$ ($1.3\%/^{\circ}\text{C}$) and ρ_1 (~ 0.25). We are now setting up a Fresnel rhomb quarter-wave system for the circular depolarization measurement.

2.4 Conclusions and Future Plans

In order to carefully study the temperature effect on the depolarization ratio of water in the OH stretching region, an improved back-scattering Raman spectrometer has been constructed. Preliminary measurements indicate that our results on the Raman spectra and depolarization ratios are in excellent agreement with most recently published data. With the completion of the minicomputer data acquisition system, which will upgrade the accuracy and the efficiency of the data acquisition, the effect of variations in the sea water compositions,

particulates concentration, organic and inorganic contaminations and variations in both laser and Raman wavelengths on the temperature sensitivities of both the two-color and cross-polarization (linear, circular and elliptical) schemes will be investigated in sufficient detail such that a parametric model for temperature measurements will be presented.

3. FIELD PERFORMANCE OF RAMAN SYSTEM

In this section we show that the cross-polarized technique for temperature measurement shows much greater promise, considering the effects of transmission through seawater, than the two-color method. Predictions of the Raman intensity detected from boat and aircraft are given, along with the statistical effects on temperature precision. Also, the effect of depolarization by scattering is estimated.

3.1 Tuning for Two-color Radiometer

Measurement of water temperature by means of a two-channel radiometer requires that the relative intensity of the Raman radiation from the water sample be measured in the two channels to a precision of the order of 1% for a temperature precision of 1°C. In addition to accurate relative calibration of the two channels of the radiometer, the relative transmission for the two channels of the medium between the water sample and the radiometer must be known or controlled to high precision. In the two-color scheme, this would generally be accomplished by tuning the laser transmitter so that the water transmission is equal at the two Raman wavelengths, i. e., so that they are centered about the wavelength of maximum transmission. This could be achieved to the necessary precision in the case of short (<1 m) path lengths through a closed system containing carefully filtered water. However, measurement of temperature to depths of 10-40 m at variable locations in the ocean would require spectral tuning of the Raman system to a degree which could not be achieved in practice.

The ratio of the intensities received by a two-color radiometer from a depth x may be written

$$\frac{I(\lambda_1)}{I(\lambda_2)} = f(T, S) e^{-[K(\lambda_1) - K(\lambda_2)]x} \quad (11)$$

The Raman scattering process is described by $f(T, S)$ which is a function of the temperature and salinity at depth x . The mistuning effect is determined by $K(\lambda)$ the spectral attenuation coefficient of seawater for diffuse (e.g., Raman) radiation. For approximate tuning, we have

$$e^{-[K_1 - K_2]x} \approx 1 - [K_1 - K_2]x + \dots$$

Suppose that we require that mistuning introduce a temperature error no greater than 0.3°C . Then we require that

$$|K_1 - K_2|x \leq .003$$

If $x = 30\text{ m}$, then we need $|K_1 - K_2| < 10^{-4}\text{ m}^{-1}$. If $K = 0.05\text{ m}^{-1}$, then K_1 and K_2 must be equal within a tolerance of 0.2%. This would be extremely difficult in the face of variable ocean conditions.

Some indication of possible variations can be obtained from Fig. 9, which shows absorption and scattering coefficients for various components of seawater given by Jerlov¹⁷ and Hulburt¹⁸. According to Sorenson Honey and Paine¹⁹, the diffuse attenuation coefficient K is typically given in the open ocean by

$$K = a + \frac{s}{6}$$

where a and s are the coefficients for absorption and scattering, respectively. As the concentration of particulates, plankton and

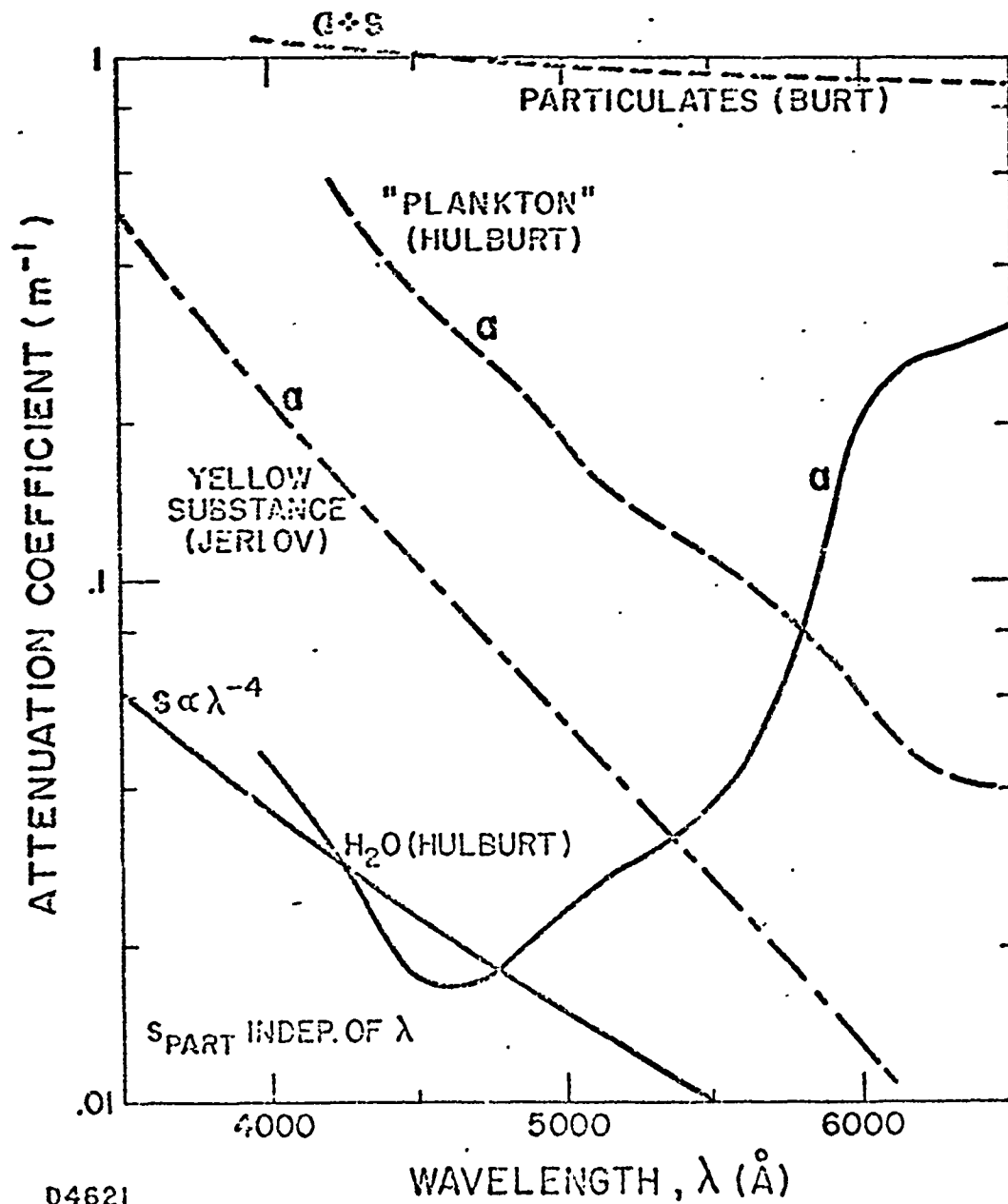


Fig. 9 Typical coefficients for scattering and absorption of light by components of sea water. 17, 18

yellow substance varies with region in the ocean, the overall function $K(\lambda)$ can be expected to vary considerably also.

3.2 Attempted Tuning via Raman Scattering

It is tempting to consider tuning for $K_1 = K_2$ by varying the laser wavelength and observing the ratio I_1/I_2 . To analyze this, let us suppose that $K(\lambda)$ has a parabolic shape:

$$K(\lambda) = \beta (\lambda - \lambda_0)^2 + \gamma$$

Substituting this function into Eq. (11), we obtain

$$\frac{I_1}{I_2} = f(T, S) e^{+2\beta (\bar{\lambda} - \lambda_0) \Delta\lambda_x} \quad (12a)$$

or, approximately,

$$\frac{I_1}{I_2} = f(T, S) (1 + 2\beta (\bar{\lambda} - \lambda_0) \Delta\lambda_x) \quad (12b)$$

Here we have used $\bar{\lambda} = (\lambda_1 + \lambda_2)/2$ and $\Delta\lambda = \lambda_2 - \lambda_1$.

Jerlov's numerical values for $K(\lambda)$ typical of his ocean Type I are plotted in Fig. 10. A least squares parabolic fit leads to $\beta = 4.3 \times 10^{-8} \text{ m}^{-1} \text{ A}^0^{-2}$ and $\gamma = 0.017 \text{ m}^{-1}$. We have plotted the exponential in Eq. (12a) and its approximation in Eq. (12b) in Fig. 11. Neither of these curves shows a feature at $\bar{\lambda} = \lambda_0$ which would show a remote observer how to tune for $K_1 = K_2$.

If the actual function $K(\lambda)$ always had a kink at its minimum, as in the case of the circles on Fig. 10, then minimum might be located by remote observation of the Raman signal. However, this is not always the case; for example, Fig. 25 of Ref. 20 shows a relatively broad, smooth $K(\lambda)$ at its minimum.

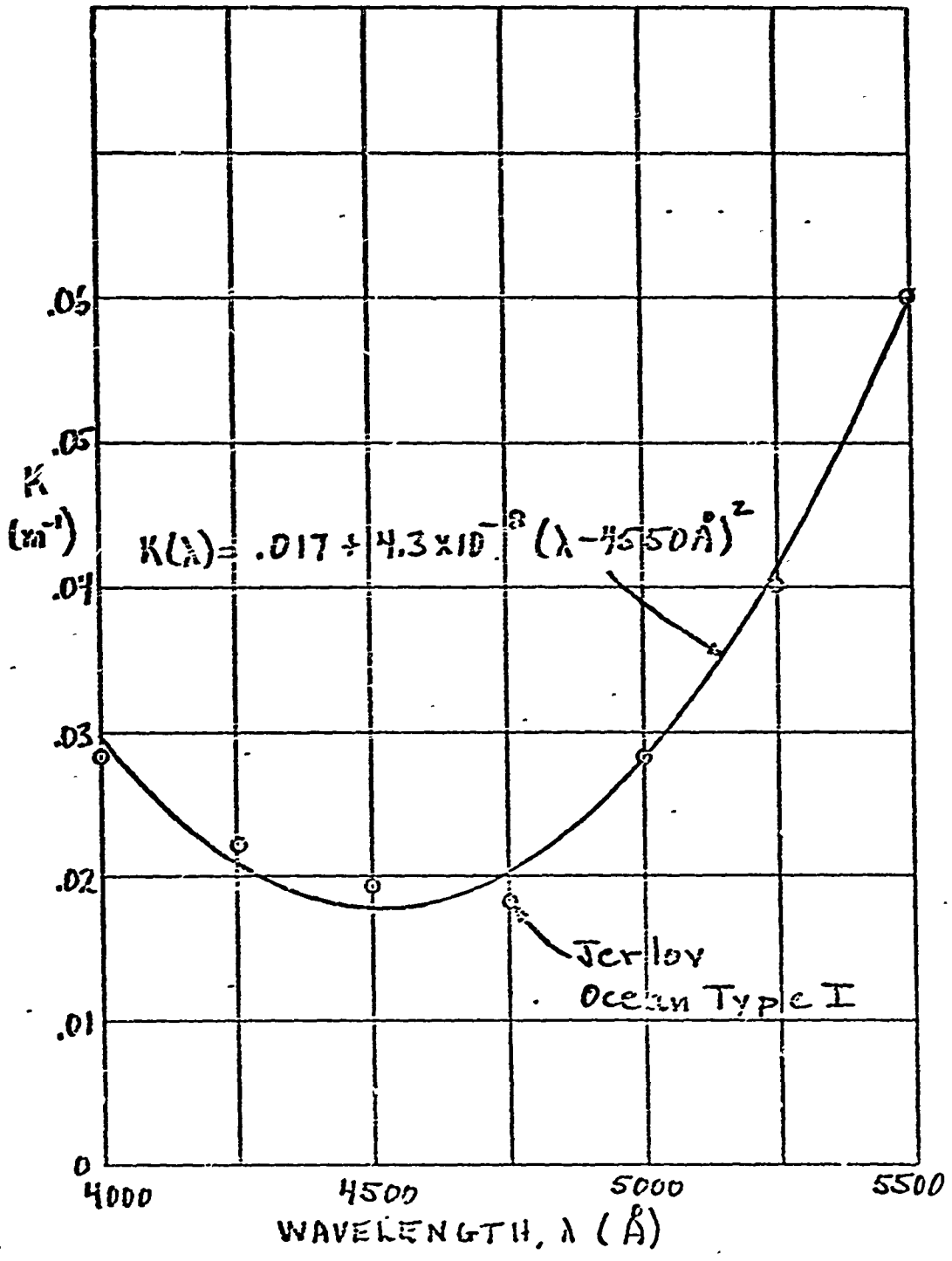


Fig. 10 Coefficient for attenuation of diffuse light according to Jerlov¹⁷ (circles) and least squares parabolic fit (curve).

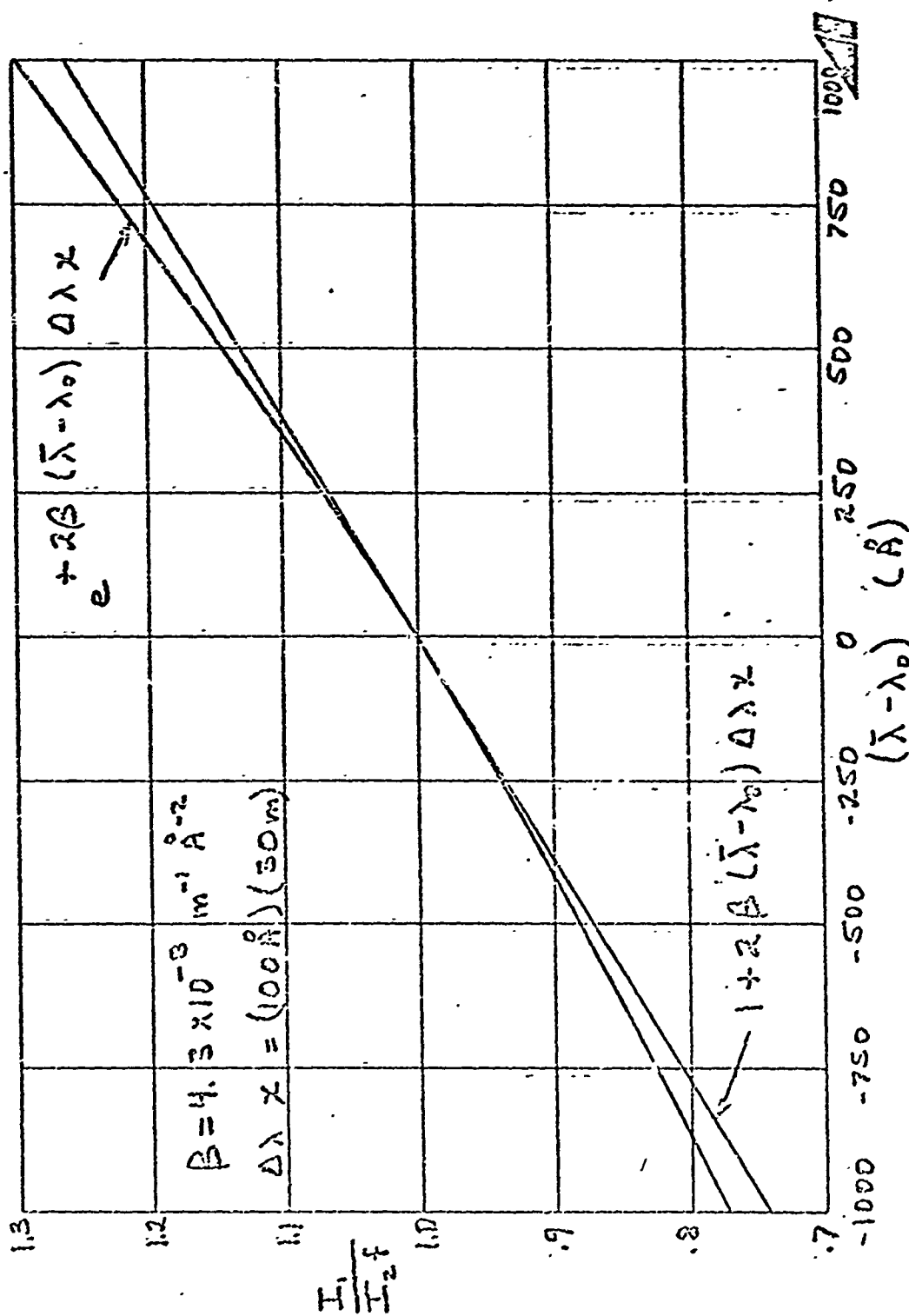


Fig. 11 Effect of spectral attenuation of sea water on Raman two-color ratio for parabolic $K(\lambda)$ (curve) and linear approximation (straight line).

3.3 Attempted Tuning Via "Rayleigh" Scattering

One might also consider tuning by observation of light scattered back to the receiver at the same wavelength as that of the laser. The difficulty with this method is that the wavelength for maximum return from depth will not generally be the same as that for maximum transmission.

If an intensity I_0 is transmitted, the irradiance received at an altitude h from a depth x would be approximately

$$H = I_0 e^{-2(a + s_f)x} s_b \Delta x / (x + h)^2, \quad (13)$$

where Δx is the thickness of the backscattering layer as determined by the length of the range gate, and a is the absorption coefficient of the seawater. Light which is scattered by an angle larger than some small angle θ_{sm} ($\sim 5^\circ$) will be lost; the coefficient for loss by this process is

$$s_f = \int_{\theta_{sm}}^{180^\circ} \sigma_\lambda(\theta) 2\pi \sin \theta d\theta \equiv s_\lambda(\theta_{sm})$$

The backscattering process can be represented by a coefficient

$$s_b = \int_{\theta_{lg}}^{180^\circ} \sigma_\lambda(\theta) 2\pi \sin \theta d\theta \equiv s_\lambda(\theta_{lg}),$$

where θ_{lg} is a large angle ($\sim 175^\circ$). $\sigma_\lambda(\theta)$ is the differential scattering coefficient ("volume scattering function") of seawater.

Although the scattering is not in fact cut off sharply at the angles θ_{sm} and θ_{lg} , this simplified treatment illustrates the major features

of the process; see Refs. 17, 18 and 21 for further discussion. The function $s_{\lambda}(\theta)$, calculated from measurements of $\sigma(\theta)$ off Bermuda, is shown in Fig. 12.

It would be possible, then, to measure the quantity

$$\frac{H(x+h)^2}{I_0 \Delta x} = e^{-2 [a_{\lambda} + s_{\lambda}(\theta_{sm})] x} s_{\lambda}(\theta_{lg}), \quad (14)$$

obtained by rewriting Eq. (13). This will not have a minimum at the same wavelength as $K(\lambda) \approx a_{\lambda} + s_{\lambda}(\theta_{sm})$, because of the wavelength dependence of the backscattering coefficient $s_{\lambda}(\theta_{lg})$. Also, $s_{\lambda}(\theta_{sm})$ and $s_{\lambda}(\theta_{lg})$ may have different wavelength dependences. Study of the function $s_{\lambda}(\theta)$, given in Fig. 12, shows that $s_{\lambda}(\theta_{sm})$ depends mostly on the values of $\sigma(\theta)$ in the ~ 5 to 15° range, while $s_{\lambda}(\theta_{lg})$ naturally depends only on $\sigma(\theta)$ at large angles. The small and large angle scatterings may be due to different components of seawater.

Nevertheless one could measure the right-hand side of Eq. (14) as a function of depth x , obtain $s_{\lambda}(\theta_{lg})$ by extrapolating to $x \rightarrow 0$, and thus determine a_{λ} and $s_{\lambda}(\theta_{sm})$. However, the quantities involved are all generally functions of depth as a result of stratification of seawater composition, which would frustrate attempts to measure a spatially averaged $K(\lambda)$ to the required accuracy discussed above.

3.4 Estimates of Raman Yield and Statistical Precision

A set of parameters for a practical Raman transmitter-receiver system, taken from Ref. 1, is given in Table 1. The number of photoelectrons detected by each photomultiplier tube in the system

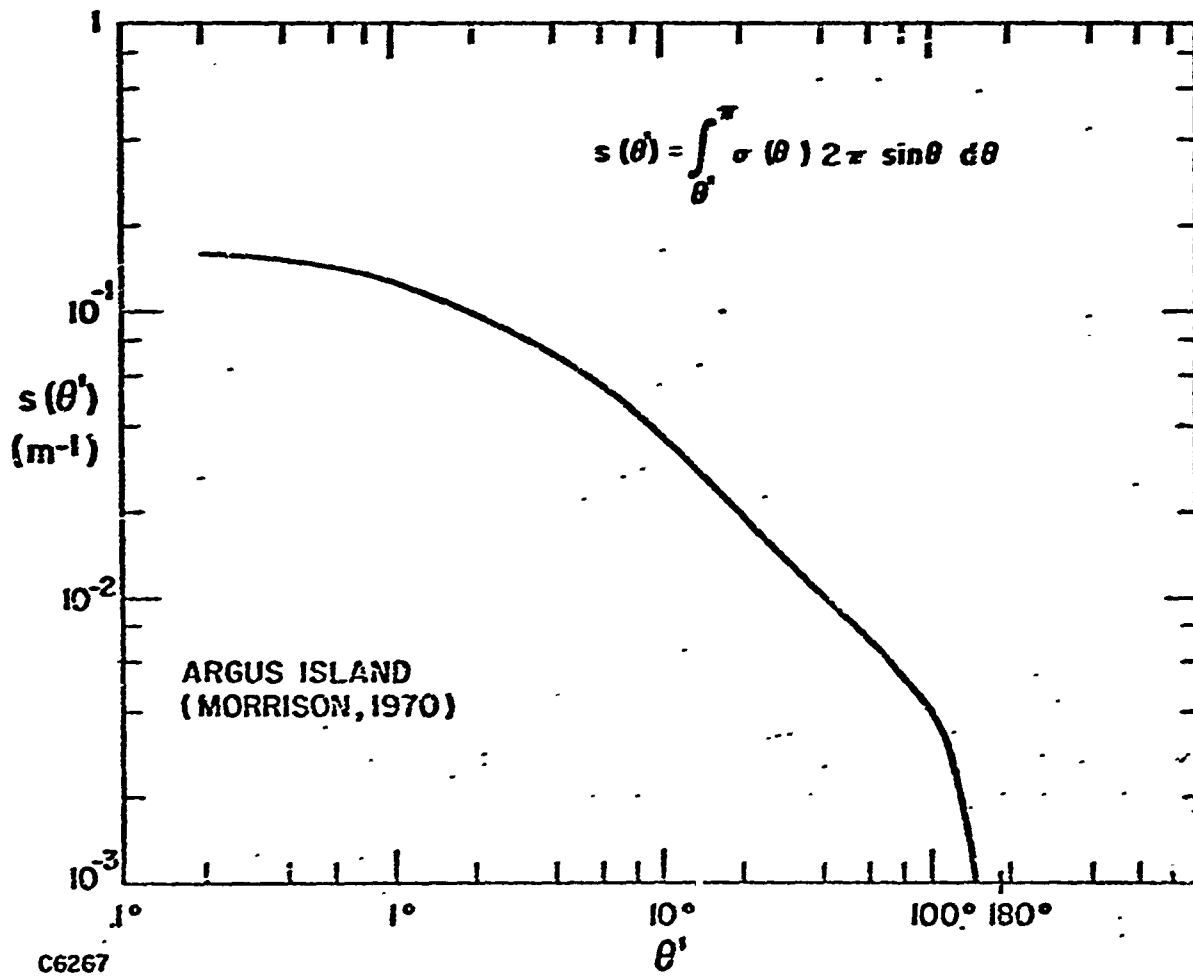


Fig. 12 Integral scattering coefficient for scatterings through angles greater than or equal to θ' .

Table 1. Parameters of Raman System

Receiver diameter (eff.)	0.3 m
Overall optical and quantum efficiency	0.03
Depth resolution	1. m
Gate duration	10^{-8} s
Receiver field of view:	
Boat	2°
Aircraft	5 m

is given by equation (6) of that reference:

$$n/E = 7.4 \times 10^{10} t_d t_u / (x+h)^2. \quad (15)$$

Here E is the transmitted laser energy (joules); t_d and t_u are the transmission of the ocean for the laser and Raman radiation respectively, and are given by Figs. 21 and 22 of Ref. 1; x is the depth of the ocean stratum sampled; and h is the height of the receiver above the ocean surface. (The latter dimensions are in meters.)

Figures 13 and 14 show the photoelectron return at a practical aircraft operating altitude of 300 m. The rms statistical error in temperature measurement is shown on the right-hand side of the figures, on the basis of 1°C -1% precision of intensity measurement. If a data sample is taken once per second (this corresponds to averaging over a distance of 100 meters if traveling at 200 knots), the 1-joule curve corresponds to an average laser power of 1 watt.

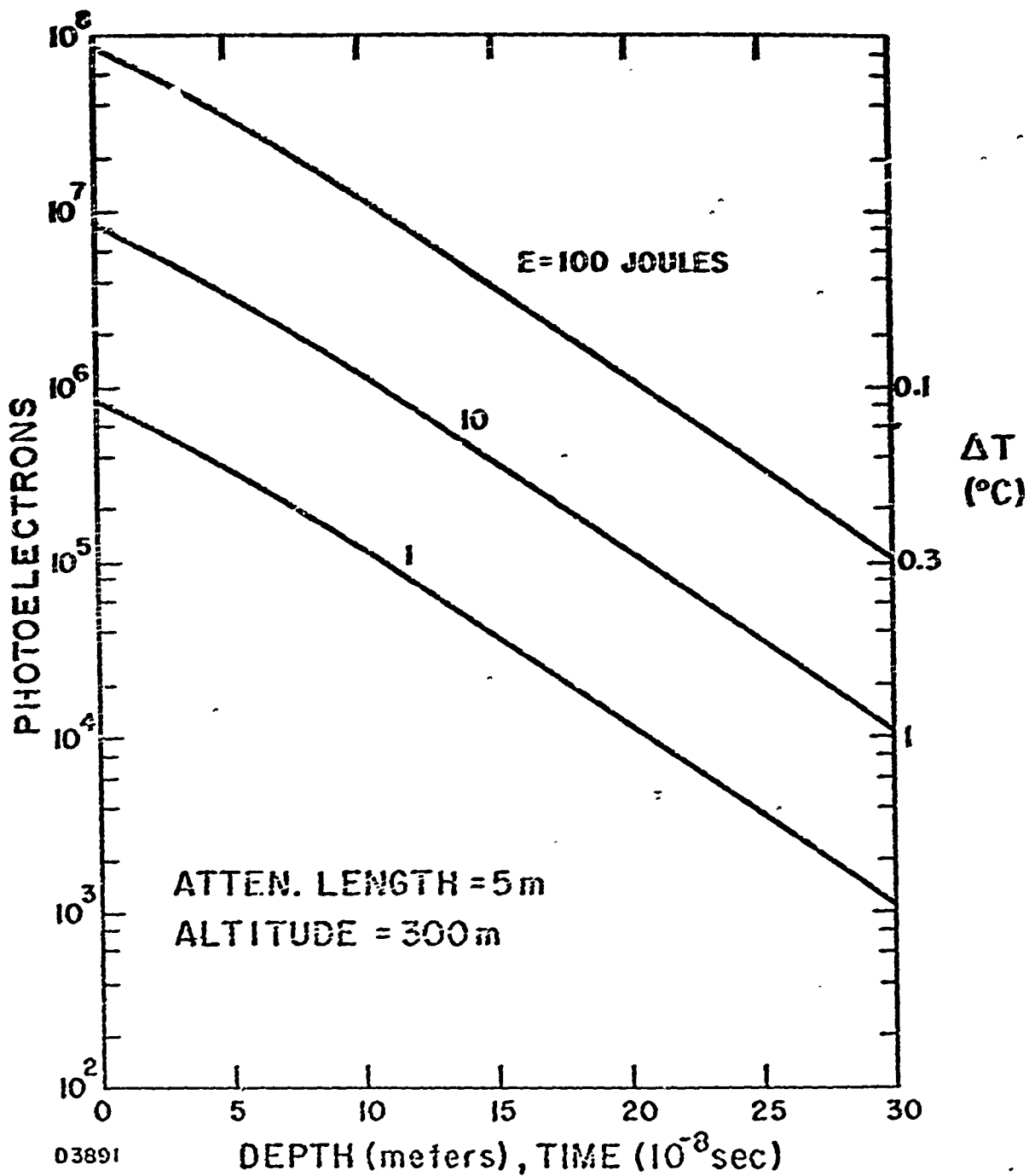
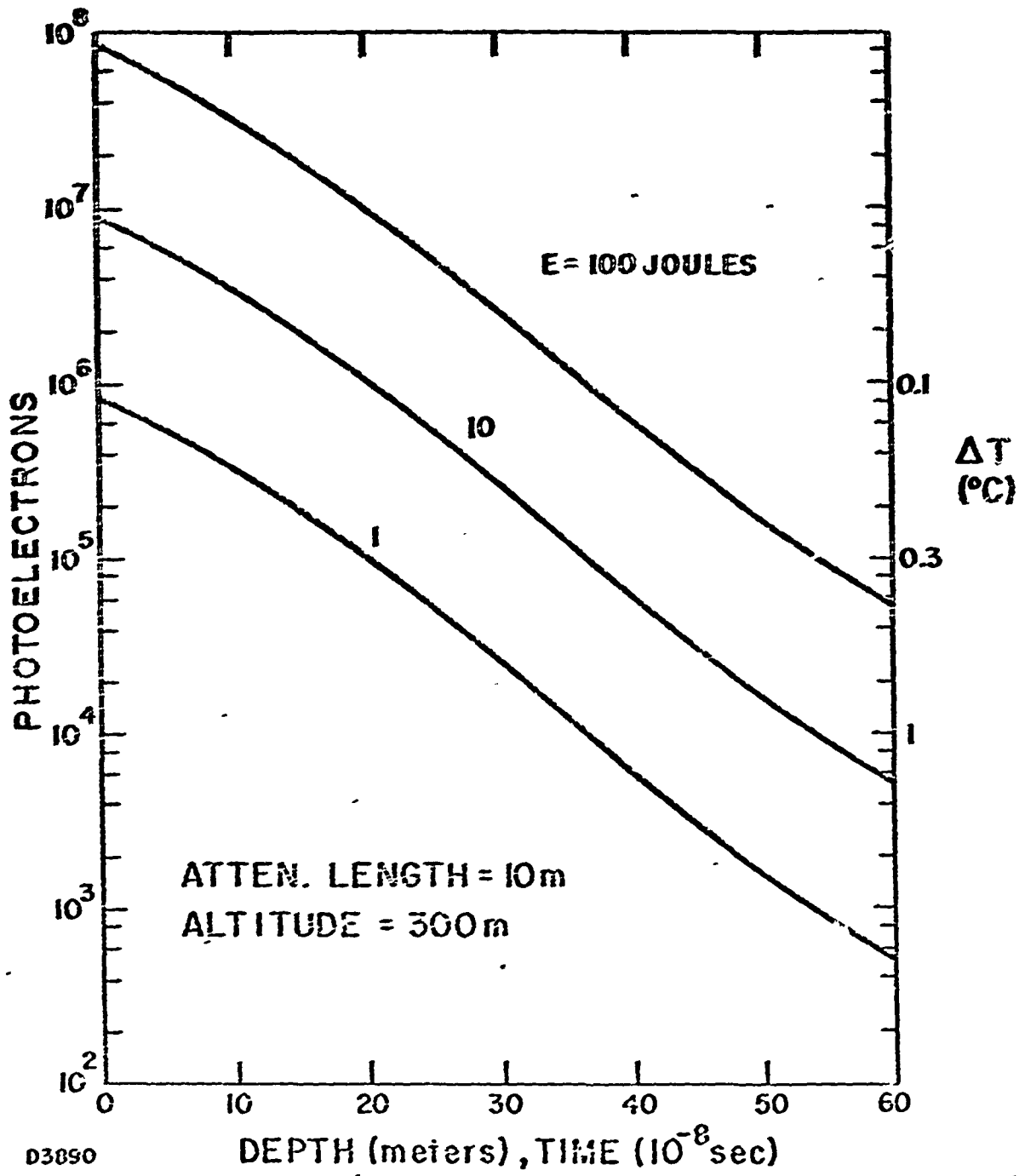


Fig. 13 Raman return at aircraft (left-hand scale) and corresponding rms statistical temperature error (right-hand scale) for attenuation length of 5 meters.



D3890

Fig. 14 Raman return at aircraft (left-hand scale) and corresponding rms statistical temperature error (right-hand scale) for attenuation length of 10 meters.

For initial field testing of the Raman technique direct simultaneous measurement of seawater temperature by means of a thermistor chain would be necessary, but integration of signals over a longer period of time would be possible. These factors point to a boat-mounted Raman system. The expected return is shown on Fig. 15. One joule (e. g., 0.07 watt integrated for 14 sec) would be sufficient here.

3.5 Depolarization by Small-Angle Scattering

The laser transmitter output can be depolarized not only by Raman scattering but also by small-angle scattering in the ocean. The latter effect can change the $\rho - T$ calibration curve.

Experiments have been performed to assess the magnitude of depolarization by small-angle scattering. The scattering medium was a suspension of sediment from locally available loam. Heavier particles were allowed to settle out for 10 minutes and then the suspension was decanted. The experimental arrangement, sketched on page A-7, included a tungsten lamp, Polaroid HCP 37 circular polarizers, an interference filter with 5670-5860 \AA band pass, and a radiometer with silicon detector. No collimating lens was used, so the intensity was attenuated as

$$I = I_0 e^{-Kx} \quad (16)$$

where K is the coefficient for attenuation of diffuse light. The diffuse

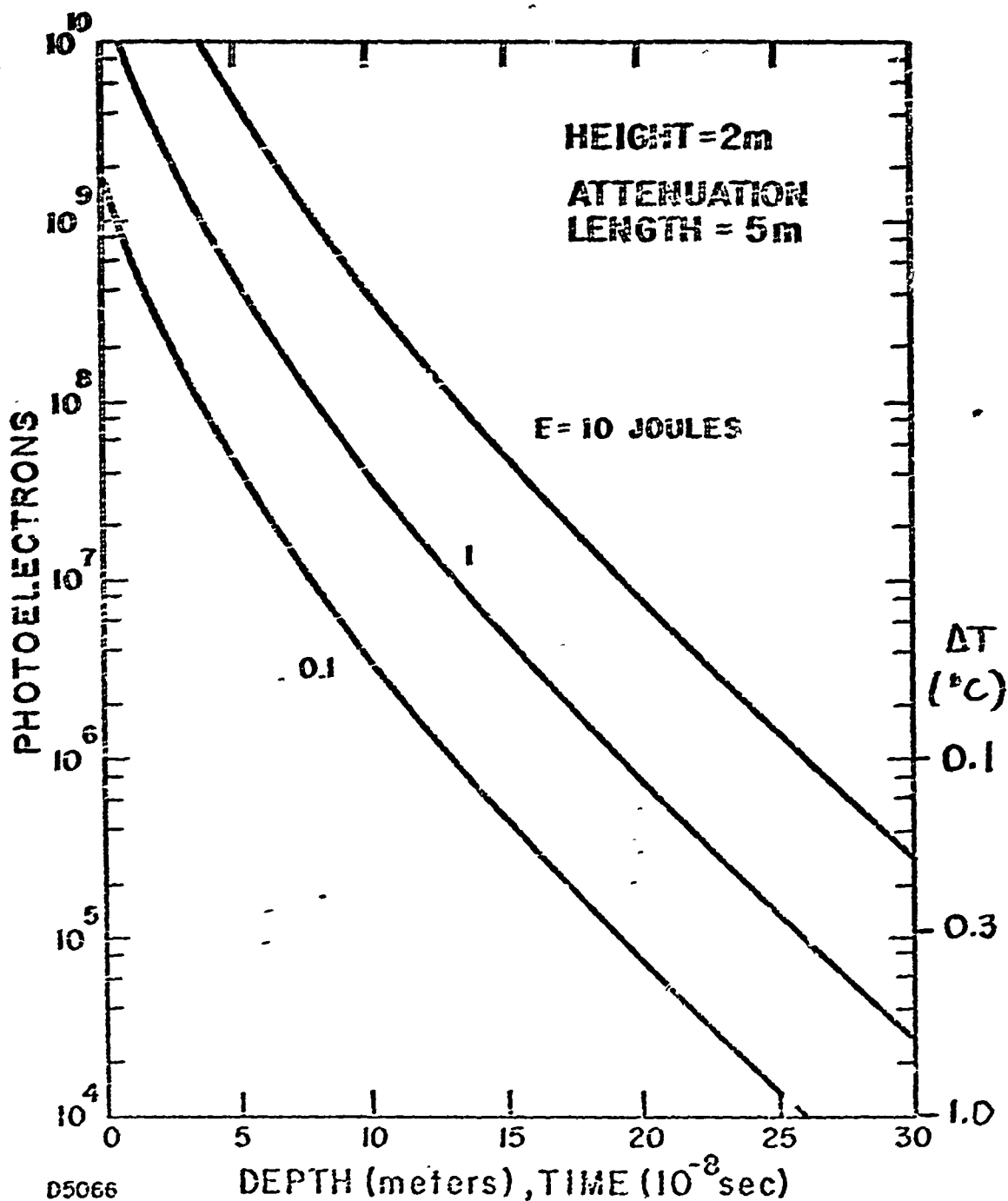


Fig. 15 Raman return at boat (left-hand scale) and corresponding rms statistical temperature error (right-hand scale) for attenuation length of 5 meters.

attenuation length Kx , determined from Eq. (16), was found to be closely proportional to the concentration of sediment as shown in Fig. 16. We also measured $I_{\perp} / I_{\parallel}$, the ratio of intensities transmitted by opposed and like circular polarizers at the ends of the water tank. The scattering depolarization ratio was calculated from

$$\rho_s = I_{\perp} / I_{\parallel} - E,$$

and plotted in Fig. 17 (See Appendix and Eq. A-6 for derivation and discussion). The extinction ratio of the polarizers was 0.0055. The depolarization ratio was found to be proportional to the attenuation length above the residual value $\rho_s = 0.005$ which is due to incomplete filtering of the water originally used.

The results can be represented by the equation $\rho_s = 0.006 Kx$. Let assume that this is also valid for the ocean, for which the relationship $K = \alpha/2$ is typical. This gives $\rho_s = 0.003 \alpha x$. From Eq. (A-2) in the Appendix the overall depolarization ratio is

$$\begin{aligned} \rho &= \rho_R + 2\rho_s (1 - \rho_R^2) \\ &= \rho_R + 2(.003) \alpha x (1 - .7^2) \\ &= \rho_R + .003 \alpha x. \end{aligned}$$

The effect of small-angle scattering is

$$\frac{1}{\rho_R} \frac{d\rho}{d(\alpha x)} = \frac{.003}{.7} = .0043.$$

Thus each attenuation length for collimated light (αx unit) affects the

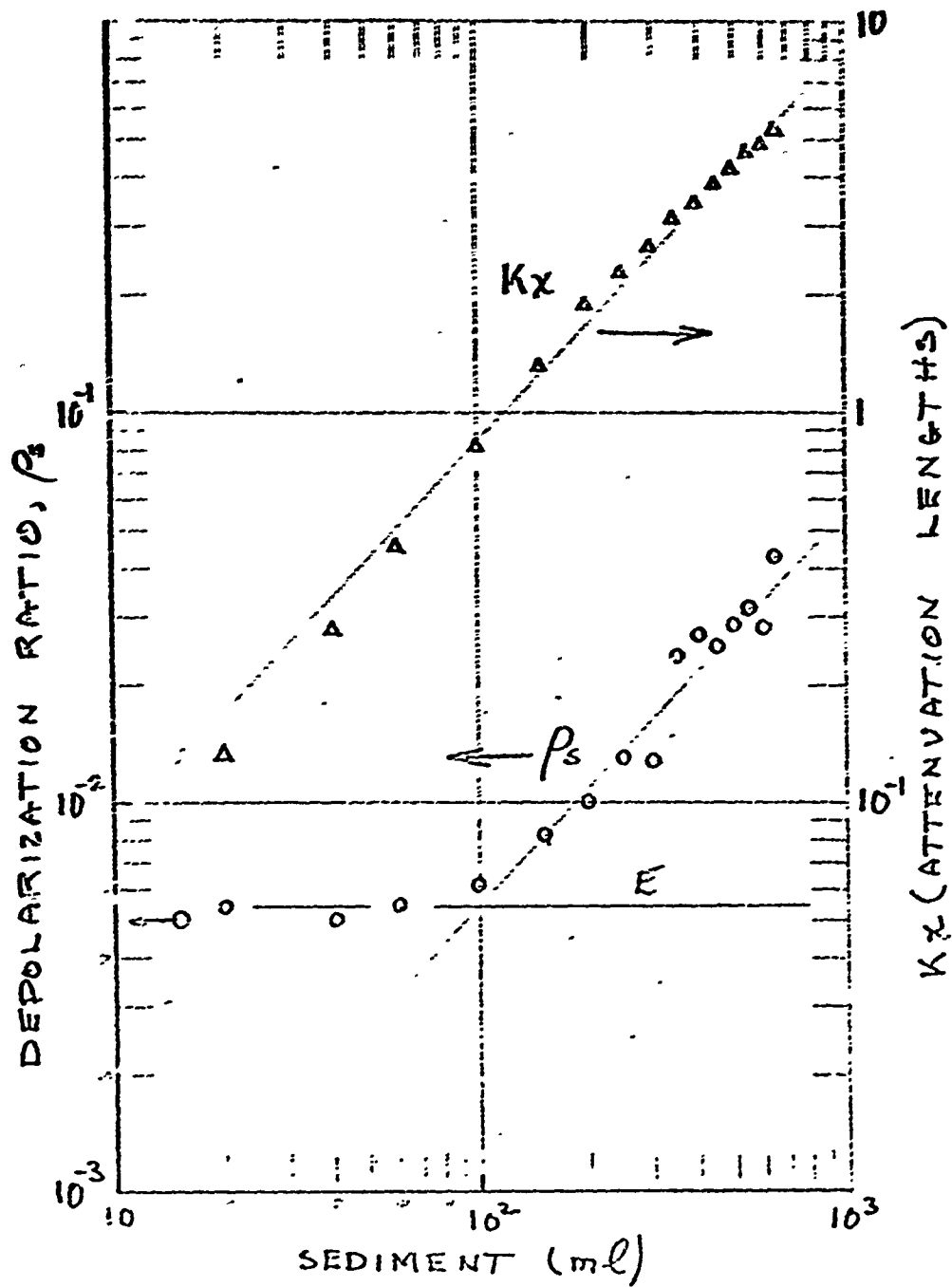


Fig. 16 Depolarization ratio (left-hand scale) and product of attenuation coefficient and path length (right-hand scale) for light vs. concentration of sediment in water. The horizontal line shows the extinction ratio of the polarizers used.

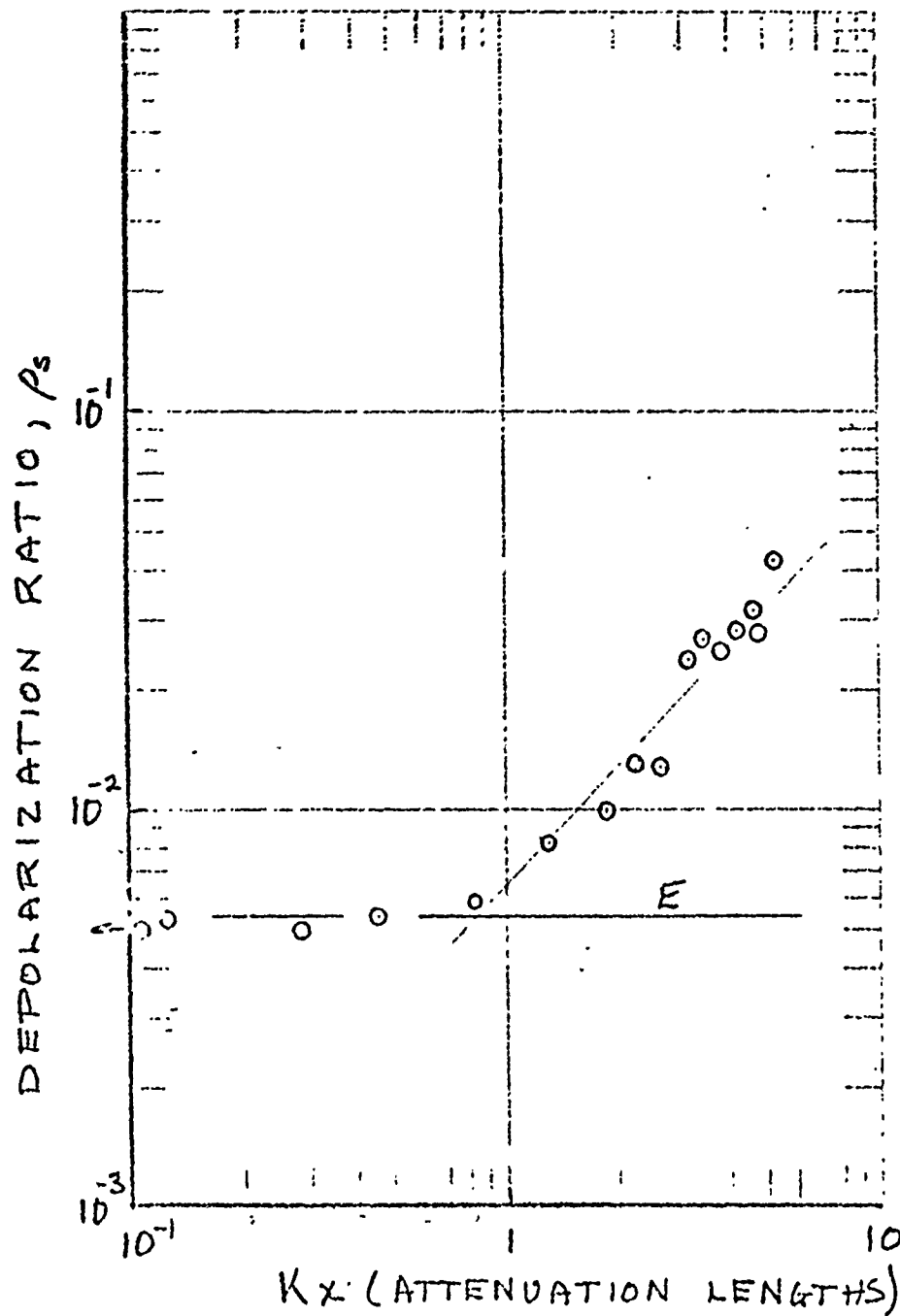


Fig. 17 Depolarization ratio
for scattering in water
vs. number of
attenuation lengths.

depolarization ratio by about 1/2% or the temperature determination by 1/2° C.

Thus precision temperature measurement will require correction for scattering effects. This will be simple to do provided that the proportionality constant between ρ and αx is independent of ocean location, because measurement of the Raman intensity will give a measure of αx . Measurements of the relationship between ρ_s and attenuation are evidently required in various seawater types.

4. FUTURE PLANS

During the remainder of the present contract we plan to perform the following:

1. Finish checking out program for minicomputer for automated data recording and monochromator control.
2. Make systematic measurements of depolarization of NaCl solutions for circularly polarized light as functions of Raman wavelength, temperature and salinity.
3. Analyze this data to determine the wavelength interval over which the depolarization ratio gives the most sensitive measure of temperature, for a given number of photoelectrons in the entire Raman spectrum, and is minimally sensitive to salinity variations.
4. Measure the Raman depolarization ratio at fixed wavelength and salinity for small temperature increments (1) to demonstrate the ability to measure temperature precisely and (2) to investigate any nonlinearities in the $\rho - T$ relationship.
5. Measure Raman spectra of natural seawater samples, looking for anomalies such as fluorescence.
6. Perform further measurements of the depolarization of circularly polarized light by small-angle scattering in natural and artificial suspensions.
7. Prepare for measurement of depolarization in coastal waters. Performance of these measurements is contingent upon boat availability.

8. Make further studies of Raman instrumentation for field use, especially concerning the availability of polarizers and spectral filters of large area and wide angular acceptance.

REFERENCES

1. C. H. Chang and L. A. Young, "Seawater Temperature Measurement from Raman Spectra", Avco Everett Research Laboratory Research Note 920 (July 1972).
2. G. E. Walrafen, *J. Chem. Phys.* 55, 768 (1971).
3. S. P. S. Porto, *J. Opt. Soc. Amer.* 56, 1585 (1966).
4. James R. Scherer, S. Kint and G. F. Bailey, *J. Mol. Spectrosc.* 39, 146 (1971).
5. W. F. Murphy and H. J. Bernstein, *J. Phys. Chem.* 76, 1147 (1972).
6. (a) J. W. Schultz and D. F. Hornig, *J. Phys. Chem.* 65, 2131 (1961); (b) K. M. Cunningham, P. D. Thesis, Yale University (1972).
7. (a) J. A. Pople, *Proc. Roy. Soc. Ser. A205*, 163 (1951); (b) T. T. Wall and D. F. Hornig, *J. Chem. Phys.* 43, 2079 (1965); (c) M. Falk and T. A. Ford, *Can. J. Chem.* 44, 1699 (1966); (d) E. U. Franck and K. Roth, *Discuss. Faraday Soc.* 43, 108 (1967).
8. (a) H. S. Frank and W. Y. Wen, *Discuss. Faraday Soc.* 24, 133 (1957); (b) L. Pauling, "Nature of Chemical Bond", Cornell University Press, Ithaca, New York, (1960), P. 464.
9. J. Liebermann, *Acoust. Soc. Amer.* 28, 1253 (1956).
10. W. K. Thompson, A. Senior and B. A. Pethica, *Nature* 211, 1086 (1966).
11. (a) J. D. Worley and I. M. Klotz, *J. Chem. Phys.* 45, 2868 (1966); (b) W. A. P. Luck and W. Ditter, *J. Phys. Chem.* 74, 3687 (1970); (c) W. C. McCabe, S. Subramanian and H. F. Fisher, *J. Phys. Chem.* 74, 4360 (1970).
12. (a) G. E. Walrafen, *J. Chem. Phys.* 47, 114 (1967); (b) G. E. Walrafen, *J. Chem. Phys.* 48, 244 (1968).
13. (a) G. E. Walrafen, *J. Chem. Phys.* 44, 1546 (1966); (b) G. Scatchard, G. M. Kavanagh and L. B. Ticknor, *J. Amer. Chem. Soc.* 74, 3715 (1952).
14. G. E. Warafen, *J. Chem. Phys.* 40, 3249 (1964).

15. L. A. Woodward, in Raman Spectroscopy , edited by H. A. Szymanski, Plenum Press, New York (1970), Vol. 2, P.1.
16. (a) G. Placzek, in Handbuch der Radiologie edited by E. Marx, Akademische Verlagsgesellschaft, Leipzig (1934), Vol. VI, 2, P.205.
(b) G. Herzberg Infrared and Raman Spectra of Polyatomic Molecules , D. Van Nostrand Company, Princeton (1945), P. 248.
17. N. G. Jerlov, Optical Oceanography (Elsevier, Amsterdam, 1969).
18. E. O. Hulburt, J. Opt. Soc. Am. 35, 698 (1945).
19. G. P. Sorenson, R. C. Honey and J. R. Paine, Stanford Research Institute, unpublished results (1966).
20. J. E. Tyler and R. C. Smith, Measurements of Spectral Irradiance Underwater (Gordon and Breach, New York, 1970).
21. L. A. Young, "Scattering of Collimated Light in the Sea", Avco Everett Research Laboratory AMP 330 (August, 1971).

APPENDIX

Depolarization by small-angle scattering

In the following analysis the action of various components upon unpolarized or polarized light will be represented by 2×2 matrices. This scheme is valid under the following assumptions: (1) In the case of linearly polarized light, no rotational features are introduced. (2) In the case of circularly polarized light, no azimuthal asymmetries are introduced. (Thus only unpolarized light is incident upon any circular polarizer. Also, any circular analyzer, which converts circularly polarized light to linear, is to be followed only by a detector which is equally sensitive to all orientations of linear polarization.)

Unpolarized or partially polarized light will be represented by two components: I_1 and I_2 . These may represent either the horizontal and vertical linear polarization components, or right- and left-hand components of circularly polarized light. The total intensity is $I = I_1 + I_2$, provided that the components are uncorrelated.

The radiation represented by this formalism is actually a mixture of polarized and unpolarized light, having intensities I_p and I_u , respectively. In the representation as two polarized components, the larger component is $I_1 = I_p + \frac{1}{2} I_u$ while the smaller is $I_2 = \frac{1}{2} I_u$.

A. 1 Depolarizing medium

Consider a medium characterized by a depolarization ratio ρ . If the incident and transmitted light are represented by the vectors (I_1, I_2) and (I_1', I_2') , we have in matrix notation

$$\begin{bmatrix} I_1' \\ I_2' \end{bmatrix} = \frac{1}{1+\rho} \begin{bmatrix} 1 & \rho \\ \rho & 1 \end{bmatrix} \begin{bmatrix} I_1 \\ I_2 \end{bmatrix} \quad (\text{A-1})$$

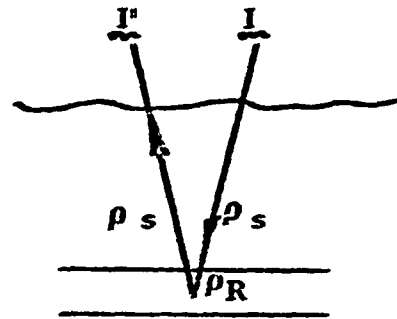
or, more compactly,

$$\underline{I}' = \underline{D} \underline{I},$$

in which \underline{D} is the depolarization matrix. From Eq. (A-1) we see that $I_1' + I_2' = I_1 + I_2$ (attenuation in the medium is neglected here). Also, if $I_2 = 0$, then $\rho = I_2'/I_1'$,

It should be pointed out that the depolarization process generates not polarized light I_2' , but unpolarized light of intensity $I_u = 2 I_2'$; the truly polarized light has intensity $I_p = I_1' - I_2'$.

Passage through successive media can be represented by the multiplication of matrices. In the sketch we show initially polarized light $\underline{I} = (I_1, 0)$ which is first depolarized by small-angle scattering in seawater (depolarization ratio ρ_s), then Raman back-scattered with a depolarization ratio ρ_R in a submerged layer, and depolarized further by scattering on the way to the surface. The overall process is described by the matrix product



$$I' = D_s D_R D_s I,$$

where D_s and D_R are the matrices for depolarization in small-angle and Raman scattering respectively. The product of the three matrices is

$$D_s D_R D_s =$$

$$\frac{1}{(1+\rho_s)^2 (1+\rho_R)} \begin{bmatrix} 1 & \rho_s \\ \rho_s & 1 \end{bmatrix} \begin{bmatrix} 1 & \rho_R \\ \rho_R & 1 \end{bmatrix} \begin{bmatrix} 1 & \rho_s \\ \rho_s & 1 \end{bmatrix} =$$

$$\frac{1}{(1+\rho_s)^2 (1+\rho_R)} \begin{bmatrix} 1 + 2\rho_R \rho_s + \rho_s^2 & 2\rho_s + \rho_R + \rho_R \rho_s^2 \\ \rho_R + 2\rho_s + \rho_R \rho_s^2 & 1 + 2\rho_R \rho_s + \rho_s^2 \end{bmatrix}$$

(Losses due to attenuation or geometrical factors are not included here.)

The overall depolarization ratio for the process is

$$\rho = \frac{I_2'}{I_1'} = \frac{\rho_R + 2\rho_s + \rho_R \rho_s^2}{1 + 2\rho_R \rho_s + \rho_s^2},$$

where we used the fact that $I_2 = 0$. Consideration that $\rho_R = O(1)$, $\rho_s \ll \rho_R$ and $\rho_s \ll 1$ leads to

$$\begin{aligned}
\rho &\cong \frac{\rho_R + 2\rho_s}{1 + 2\rho_R \rho_s} \\
&\cong \rho_R + 2\rho_s (1 - \rho_R^2 - 2\rho_R \rho_s) \\
&\cong \rho_R + 2\rho_s (1 - \rho_R^2). \tag{A-2}
\end{aligned}$$

The latter expression is sufficiently accurate for our needs.

The factor 2 appearing there arises from depolarization in both the downward and upward paths; each of them is equally important.

A.2 Polarizers and analyzers

To measure ρ_s we must use polarizers and analyzers of finite performance. The effect of a polarizer which converts unpolarized light directly into polarization component No. 1, or an analyzer which passes primarily component No. 1, is represented by the equation

$$\begin{bmatrix} I_1' \\ I_2' \end{bmatrix} = \begin{bmatrix} t & 0 \\ 0 & c \end{bmatrix} \begin{bmatrix} I_1 \\ I_2 \end{bmatrix}, \tag{A-3}$$

or

$$I_m' = P_{m1} I_m$$

In the case of a polarizer or analyzer for the second component, we have

$$\begin{bmatrix} I_1' \\ I_2' \end{bmatrix} = \begin{bmatrix} e & 0 \\ 0 & t \end{bmatrix} \begin{bmatrix} I_1 \\ I_2 \end{bmatrix} \quad (A-4)$$

or

$$I' = P_2 I$$

In the above, t is the transmission of the polarizer for the "passed" component, and e ("extinction") is the transmission for the "blocked" component.

The combination of a polarizer and analyzer both for component 1 is represented by the matrix

$$P_1^2 = \begin{bmatrix} t & 0 \\ 0 & e \end{bmatrix} \begin{bmatrix} t & 0 \\ 0 & e \end{bmatrix} = \begin{bmatrix} t^2 & 0 \\ 0 & e^2 \end{bmatrix}$$

If unpolarized light, for which $I_1 = I_2 = \frac{1}{2} I$, is incident upon the combination, the transmitted intensity is

$$\begin{aligned} I_{11} &= (I_{11})_1 + (I_{11})_2 = t^2 I_1 + e^2 I_2 \\ &= \frac{1}{2} (t^2 + e^2) I = \frac{1}{2} t^2 I. \end{aligned}$$

The latter approximation is accurate to second order because $e \ll t$.

For a polarizer and analyzer each for component 2 we also obtain

$$I_{11} = \frac{1}{2} t^2 I.$$

If the analyzer is crossed to the polarizer (e. g., vertical vs. horizontal, or left-hand vs. right-hand), the transmission matrix is

$$\underset{w}{P_1} \underset{w}{P_2} = \begin{bmatrix} t & 0 \\ 0 & e \end{bmatrix} \begin{bmatrix} e & 0 \\ 0 & t \end{bmatrix} = \begin{bmatrix} te & 0 \\ 0 & te \end{bmatrix} = \underset{w}{P_2} \underset{w}{P_1}$$

(All diagonal matrices commute.) The intensity of originally unpolarized light transmitted is

$$I_1 = (I_1)_1 + (I_1)_2 = teI_1 + teI_2 = teI$$

The extinction ratio of the polarizer-analyzer combination may be defined as

$$E = I_1 / I_{11},$$

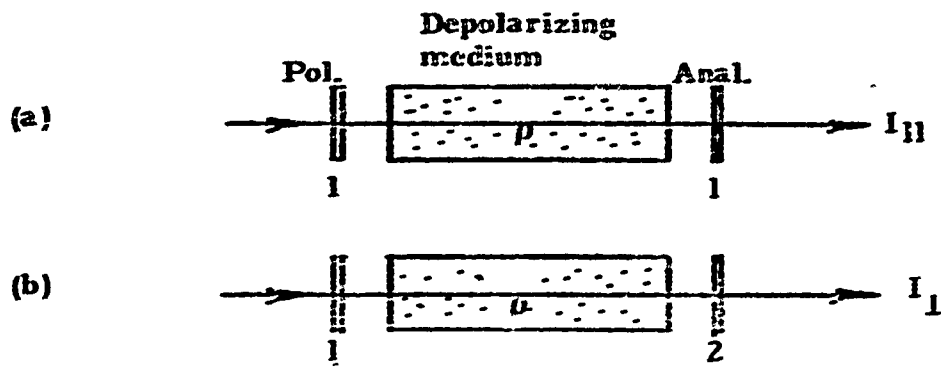
which leads to

$$E = 2e/t. \tag{A-5}$$

A. 3 Depolarization measurements

In measurements of the depolarization ratio for a scattering medium, a correction may be necessary for the finite extinction ratio of the polarizer and analyzers. The sketch shows two configurations:

(a) with polarizer and analyzer of the same type, which transmit intensity I_{11} , and (b) with crossed polarizer and analyzer which transmit intensity I_1 . The transmission matrix for case (a) is



$$\begin{aligned}
 \frac{P_1}{w} \quad \frac{D}{w} \quad \frac{P_1}{w} &= \begin{bmatrix} t & 0 \\ 0 & e \end{bmatrix} \frac{1}{1+\rho} \begin{bmatrix} 1 & \rho \\ \rho & 1 \end{bmatrix} \begin{bmatrix} t & 0 \\ 0 & e \end{bmatrix} \\
 &= \frac{1}{1+\rho} \begin{bmatrix} t^2 & \rho t e \\ \rho t e & e^2 \end{bmatrix} ;
 \end{aligned}$$

for case (b) it is

$$\begin{aligned}
 \frac{P_2}{w} \quad \frac{D}{w} \quad \frac{P_1}{w} &= \begin{bmatrix} e & 0 \\ 0 & t \end{bmatrix} \frac{1}{1+\rho} \begin{bmatrix} 1 & \rho \\ \rho & 1 \end{bmatrix} \begin{bmatrix} t & 0 \\ 0 & e \end{bmatrix} \\
 &= \frac{1}{1+\rho} \begin{bmatrix} t e & \rho e^2 \\ \rho t^2 & t e \end{bmatrix} .
 \end{aligned}$$

If the incident light is unpolarized ($I_1 = I_2$), the transmitted intensities are

$$I_{11} = \frac{1}{2} \frac{t^2 + 2\rho t e + e^2}{1+\rho} I$$

and

$$I_1 = \frac{1}{2} \frac{\rho (t^2 + e^2) + 2 t e}{1+\rho} I .$$

Their ratio is

$$\frac{I_1}{I_{11}} = \frac{\rho (t^2 + e^2) + 2 te}{2\rho te + t^2 + e^2},$$

with which becomes, with the use of Eq. (A-5),

$$\frac{I_1}{I_{11}} = \frac{\rho (1 + E^2/4) + E}{1 + \rho E + E^2/4}.$$

We remember that $E \ll 1$. If, in addition, $\rho \ll 1$, the expression

$$\frac{I_1}{I_{11}} = \rho + E \tag{A-6}$$

is accurate to second order. If $\rho \sim O(1)$, we have $I_1 / I_{11} \sim \rho$. In general, we could define ρ as

$$\rho = \lim_{E \rightarrow 0} \frac{I_1}{I_{11}};$$

The limit implies an ideal analyzer.